ResearchGate

See discussions, stats, and author profiles for this publication at: https://www.researchgate.net/publication/349150353

Broadband topological valley transport of elastic wave in reconfigurable phononic crystal plate

Article *in* Applied Physics Letters · February 2021

DOI: 10.1063/5.0036840

CITATIONS
61

READS
934

5 authors, including:

Nan Gao
Universitat Jaume I
15 PUBLICATIONS **234** CITATIONS
SEE PROFILE

Sichao Qu
The University of Hong Kong
12 PUBLICATIONS **174** CITATIONS
SEE PROFILE

Liang Si
Zhejiang University
1 PUBLICATION **60** CITATIONS
SEE PROFILE

W. Q. Chen
Zhejiang University
658 PUBLICATIONS **17,019** CITATIONS
SEE PROFILE

Some of the authors of this publication are also working on these related projects:

Structural Analysis of Piezomagnetic/Piezoelectric layered structures View project

Room Acoustics with Metamaterials View project

All content following this page was uploaded by Nan Gao on 10 February 2021.

The user has requested enhancement of the downloaded file.

Applied Physics Letters

Broadband topological valley transport of elastic wave in reconfigurable phononic crystal plate

Cite as: Appl. Phys. Lett. **118**, 063502 (2021); https://doi.org/10.1063/5.0036840
Submitted: 10 November 2020 . Accepted: 29 January 2021 . Published Online: 09 February 2021

Nan Gao, Sichao Qu, Liang Si, Jiao Wang, and Weiqiu Chen

View Online Export Citation CrossMark

© 2021 Author(s).

AIP Publishing

Applied Physics Letters ARTICLE scitation.org/journal/apl

Broadband topological valley transport of elastic wave in reconfigurable phononic crystal plate

Cite as: Appl. Phys. Lett. **118**, 063502 (2021); doi: 10.1063/5.0036840
Submitted: 10 November 2020 · Accepted: 29 January 2021 ·
Published Online: 9 February 2021

View Online Export Citation CrossMark

Nan Gao,[1,2] Sichao Qu,[2] Liang Si,[1] Jiao Wang,[1,3,a)] and Weiqiu Chen[1,4,a)]

AFFILIATIONS

[1]Key Laboratory of Soft Machines and Smart Devices of Zhejiang Province and Department of Engineering Mechanics, Zhejiang University, Hangzhou 310027, China
[2]Department of Physics, The Hong Kong University of Science and Technology, Clear Water Bay, Hong Kong, China
[3]Department of Civil Engineering, Zhejiang University, Hangzhou 310027, China
[4]Soft Matter Research Center, Zhejiang University, Hangzhou 310027, China

[a)]**Authors to whom correspondence should be addressed:** 11524019@zju.edu.cn and chenwq@zju.edu.cn.
Tel./Fax: 86-571-87951866

ABSTRACT

Topological insulators have attracted intensive attention due to their robust properties of path defect immunity, with diverse applications in electromagnetic, acoustic, and elastic systems. The recent development of elastic topological insulators (ETIs), based on artificially structured phononic crystals, has injected new momentum into the manipulation of elastic waves. Earlier ETIs with unreconfigurable geometry and narrow frequency bandgaps hinder the exploration and design of adaptable devices. In this work, a tunable phononic crystal plate with Y-shaped prisms is designed to support valley transport of elastic waves, based on the analogy of the quantum valley Hall effect. By rotating the prisms to reconstruct the configuration, the mirror symmetry is broken to open a new bandgap. Based on this characteristic, we design an interface between two ETIs with different symmetry-broken geometries, which supports topologically protected edge states. We further design a reconfigurable device for elastic wave channel switching and beam splitting and demonstrate it both numerically and experimentally. In addition, in order to meet the requirement of the wide frequency range, the genetic algorithm is adopted to optimize the geometry so as to achieve the broadband valley transportation of elastic waves. The results obtained in this paper can promote the practical applications of tunable broadband elastic wave transmission.

Published under license by AIP Publishing. https://doi.org/10.1063/5.0036840

It is well known that there are three polarizations[1] for elastic wave propagation in infinite homogeneous materials (i.e., one is longitudinal and the other two are transverse). The complex coupling and conversion between different polarization modes under specific elastic boundary hinder the ability to manipulate elastic waves. Therefore, it is of great importance to reduce the number of modes considered and make them decoupled. For a subwavelength-thick plate, we just need to consider three zeroth-order elastic wave modes in the low-frequency regime, i.e., symmetrical Lamb mode (S_0), anti-symmetrical Lamb mode (A_0), and shear horizontal mode (SH_0). It is noticed that the out-of-plane displacement mostly dominates the A_0 mode, which can be easily excited by a vertical load applied to one surface of the plate. This serves as a precious foundation to realize topological phases in this work.

In recent years, the analogy of quantum Hall effects (QHEs), quantum spin Hall effects (QSHEs), and quantum valley Hall effects (QVHEs) to the classical electromagnetic,[2–5] acoustic,[6–12] and mechanical[13–22] systems has become a research hotspot.[13,17,23–25] In the field of condensed matter physics, QVHEs are realized by introducing angular rotation of the electron wave function at points K and K' in the first Brillouin zone (first BZ), which provides an intrinsic magnetic moment, analogous to that provided by the electron spin. Similarly, vortex chirality (i.e., pseudospin) of elastic energy flow provides a new degree of freedom for elastic waves via the orbital angular momentum, which can be realized by breaking the mirror symmetry. Based on this idea, many successful works have been demonstrated in the past few years. In elastic systems, the bandgap (where topologically protected edge states can exist) can be opened in miscellaneous ways such as introducing a difference in the mass[16,23,26,27] and/or in the stiffness,[23,26] making geometric frustration,[28,29] changing the local strain field,[30] or rotating specific components.[31–33] Among them, a discretized spring-mass system[23] can serve as a versatile platform to achieve various topological phases. However, the designed geometries

Published under license by AIP Publishing

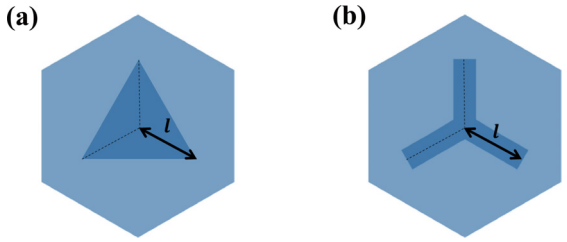

FIG. 1. Two configurations: (a) PCP with a triangular prism; and (b) PCP with a Y-shaped prism. The distance between the vertex and the center of the triangle prism in (a) is consistent with the leg length of the Y-shaped prism in (b).

of these existing elastic topological insulators (ETIs), while effective in demonstrating the topological phenomena, are unreconfigurable and with relatively narrow band characteristic that may hinder the practical application in flexible and active control of elastic waves.

To mitigate these problems, we proposed a thin phononic crystal plate (PCP) to present an analog to QVHEs by utilizing the property of A_0 mode. The PCP was constructed by arranging cylindrical prisms on both sides of a uniform plate. When designing the configuration of the PCP, we further optimized the traditional triangular prism [Fig. 1(a)] and designed a Y-shaped one [Fig. 1(b)]. Breaking the mirror symmetry could be accomplished by simply rotating the Y-shaped prism on both sides of the plate while preserving the C_3 symmetry, which leads to the opening of the Dirac point, forming a new bandgap. What needs to be emphasized here is that, the improved Y-shaped prism can have a wider bandgap than the triangular one, which also satisfies our broadband design purpose. In addition, structural optimization technology can be used to achieve the optimal working frequency range of valley transportation.[34] In order to make the broadband effect more obvious, we used the genetic algorithm[35] to further optimize the configuration of the PCP so as to broaden the bandgap where valley transport modes can be excited. The reader is referred to the supplementary material for more details about the optimization.

In this way, the two valleys (K and K') are not equivalent to each other in the reciprocal space and chiral-valley edge states are formed along the interface between two PCPs with different topological phases. Topologically protected valley transport modes are observed both numerically and experimentally, of which the robustness to defects and local disorder is verified as well. Finally, the reconfigurability of the PCP is demonstrated by constructing a "control region" where the orientation of Y-shaped prisms can be controlled. The switching of two orientation states enables the elastic waves to only propagate in the desired channel or in two channels simultaneously (i.e., a beam splitter). The proposed reconfigurable and broadband PCP provides a

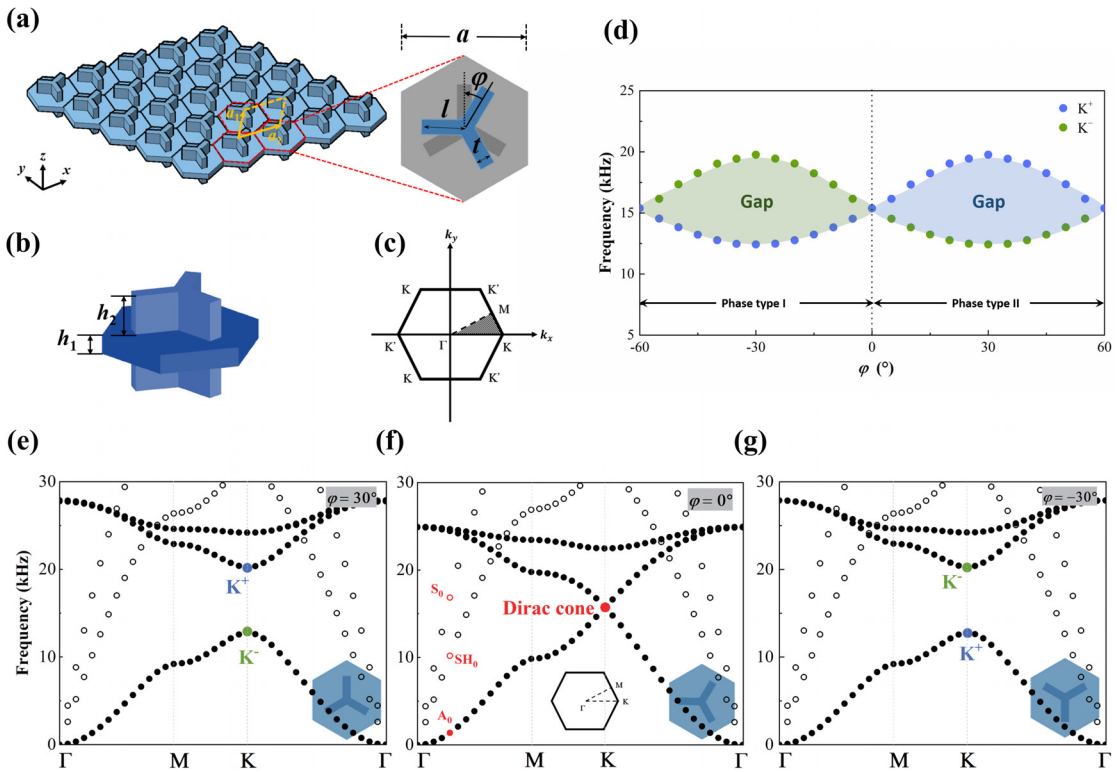

FIG. 2. PCP with Y-shaped prisms. The plate is made of aluminum with mass density $\rho_0 = 2700\,\mathrm{kg/m^3}$, longitudinal wave velocity $c_{L0} = 5091.8\,\mathrm{m/s}$, and transverse wave velocity $c_{T0} = 3110.3\,\mathrm{m/s}$. The prisms are made by stainless steel with $\rho_1 = 7903\,\mathrm{kg/m^3}$, $c_{L0} = 5264.1\,\mathrm{m/s}$, and $c_{T0} = 3239.8\,\mathrm{m/s}$. (a) The whole PCP structure; (b) unit cell of the PCP with two Y-shaped cylindrical prisms on both sides; (c) the first Brillouin zone and irreducible Brillouin zone (shadow part) of the lattice; (d) the relation between the rotation angle φ and the width of bandgap; and (e)–(g) dispersion relations with different angles $\varphi = 30^\circ$, $\varphi = 0$, and $\varphi = -30^\circ$, respectively. The symbols K^+ and K^- denote the pseudospin states.

Published under license by AIP Publishing

useful platform for elastic wave manipulation, where various future applications in integrated on-chip mechanical system,[33] structural health monitoring,[36,37] and elastic wave focusing[38] can be expected.

The unit cell of this PCP is shown in Figs. 2(a) and 2(b), where a_1 and a_2 are the basis vectors of the unit cell, a is the lattice constant, and h_1 and h_2 denote the thickness of the plate and the Y-shaped prisms, respectively. The length and width of each leg of the Y-shaped prism are l and w, respectively, and φ is the anticlockwise rotation angle of the prism. The concrete values are $a = 25$ mm, $h_1 = 0.2a$, $h_2 = 0.4a$, $l = 0.4361a$, and $t = 0.2379a$, which have been optimized by the genetic algorithm (see the supplementary material). The substrate plate is made of aluminum, and the prisms are made by stainless steel. The first BZ of the unit cell is shown in Fig. 2(c), whose shadow part is the irreducible BZ, and the band structure is scanned from the path $\Gamma - M - K - \Gamma$ around the irreducible BZ. It appears in Fig. 2(f) with $\varphi = 0°$ that in the low frequency range, there are only three dispersive curves, which are A_0, S_0, and SH_0 modes, respectively. The out-of-plane mode A_0 dominates all the band structures and is of major interest in the noncontact measurement, characterized by the parabolic dispersions. Because of the matched mirror symmetries between the lattice and triangular scatterers, the Dirac cone at the corners of first BZ is preserved [Fig. 2(f)]. By rotating the upper and lower prisms around their geometric center simultaneously, the band structure will be changed, due to the breaking of mirror symmetry. When $\varphi = 30°$ and $\varphi = -30°$, the band structures are shown in Figs. 2(e) and 2(g), respectively, where we can clearly see that a wide bandgap is opened. In fact, the rotation angle can be other values, leading to the characteristic of the tunable bandgap, as shown in Fig. 2(d).

It should be noted that in the band structure of A_0 mode, in principle, there can also exist the SH_0 and S_0 modes, as shown in Fig. 3(a). However, in the following simulations and experiments, we can just excite the z-direction displacement at the source point of the PCP to get pure A_0 mode, since the A_0 mode is easily excited separately. The finite element method (FEM) software COMSOL Multiphysics is used here to carry out the dispersion analysis. The topological mode inversion process is illustrated in Fig. 3(b), accompanied by the broken mirror symmetry. In order to get an understanding of the physical picture behind the pseudospin states, we map the elastic z-displacement,

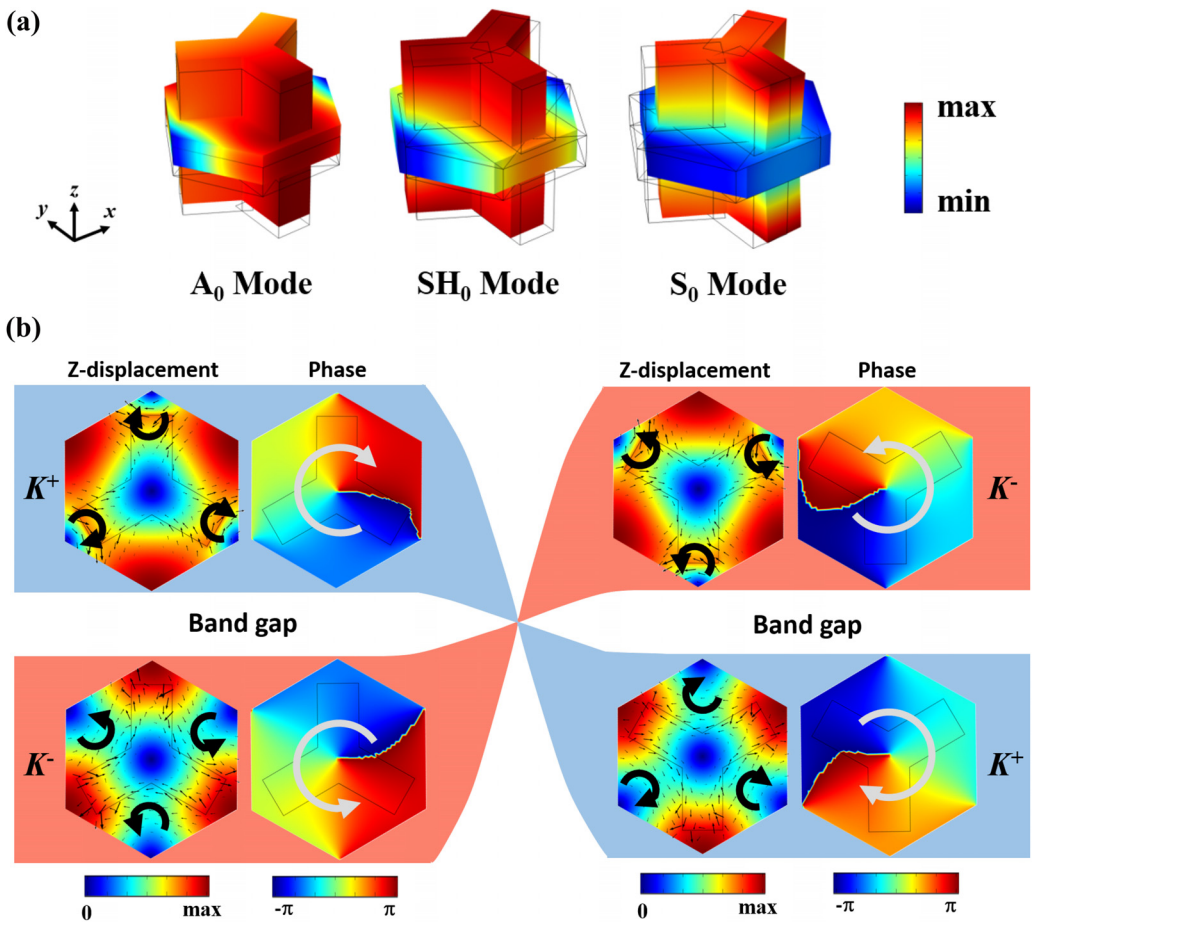

FIG. 3. Modal analysis. (a) A_0, S_0, and SH_0 modes at three points in Fig. 1(f). Rainbow color shows the displacement field and the black profile denotes the undeformed structure; (b) topological mode inversion with the transition of pseudospin states. The rainbow color shows the amplitude of the absolute value of the z-component displacement, the black arrows represent the direction of the mechanical energy flow of the elastic wave, and the gray arrows denote the direction of phase change via time.

Published under license by AIP Publishing

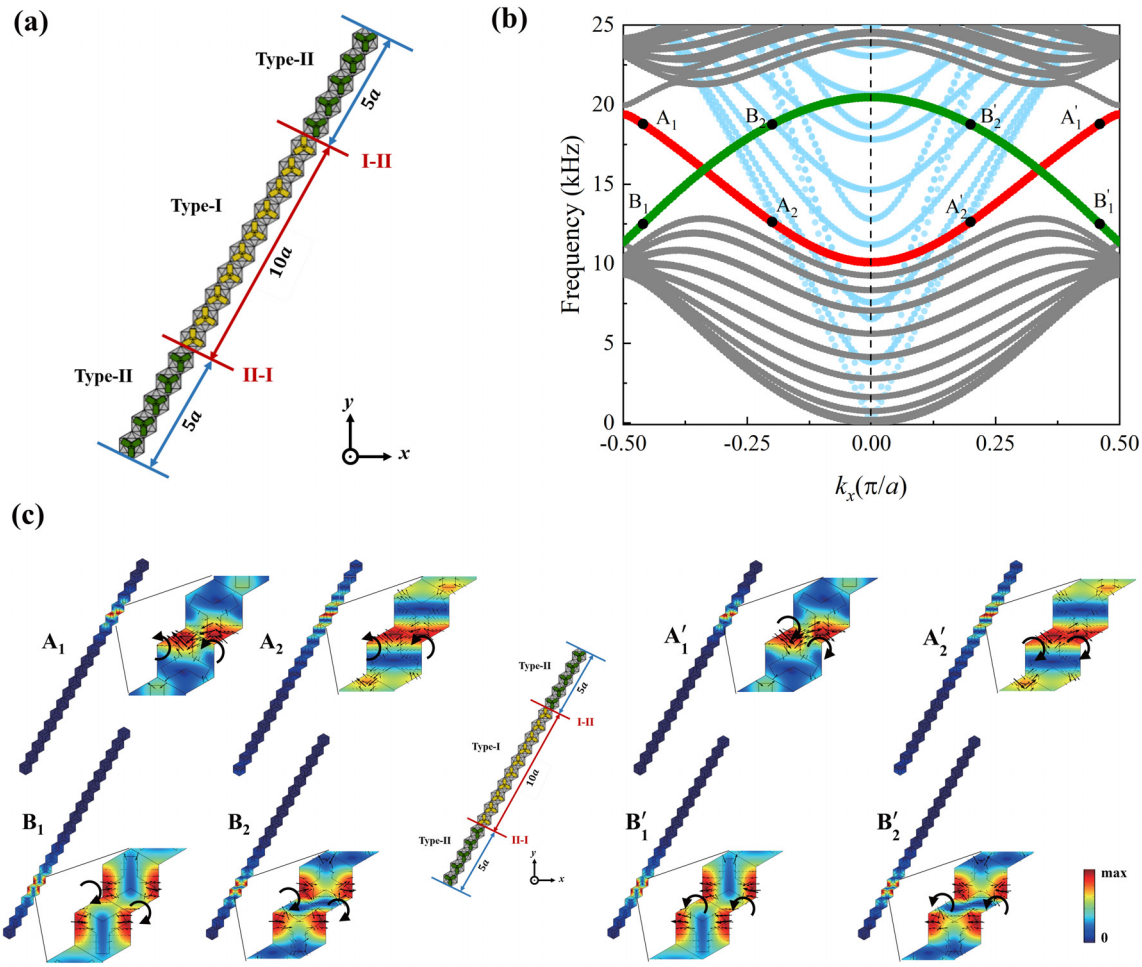

FIG. 4. Dispersion relation and modal analysis of the supercell. (a) A supercell composed of Type-I and Type-II PCs; (b) projected band structure along the ΓK direction for the supercell in (a), where blue dots are the in-plane modes, the gray dots are the out-of-plane modes, and the red and green lines denote edge states; and (c) different edge modes corresponding to points $A_{1,2}$, $A'_{1,2}$, $B_{1,2}$, and $B'_{1,2}$. The black arrows denote the direction of mechanical energy flow, which describes the spatial distribution and direction of energy flux, and in COMSOL, its component is expressed as $I_i = \frac{1}{2}\mathrm{Re}(-\sigma_{ij}v_j^*)$, where σ_{ij} is the stress component and v_j^* is the complex conjugate of the particle velocity component.

energy flow, and phase fields, as shown in Fig. 3(b). The z-direction displacement modes at the two points (K^- and K^+) are similar, but the cyclic directions of mechanical energy flow are opposite to each other, which represent the valley pseudospin modes with opposite chirality. Here, elastic valley pseudospin states (K^- and K^+) exhibit reversed chirality similar to electronic spin states. These kinds of chiral patterns are also reported in other ETIs,[4,12,33] and can be seen as an important characteristic of valley ETIs. The chirality characteristic of the Lamb wave valley mode originates from the fact that valley modes carry an intrinsic orbital angular momentum.

Next, we combine two kinds of PCPs with distinct nontrivial topological phases ($C_{K^+} = 1/2$ and $C_{K^-} = -1/2$), one being the PCP with $\varphi = 30°$ (Type-I) and the other one with $\varphi = -30°$ (Type-II), to form a supercell, as shown in Fig. 4(a), which contains two interfaces. All the boundaries of the supercell are applied with Bloch periodic boundary. The projection of the band structure along the ΓK direction is shown in Fig. 4(b), where the blue and gray dots represent the in-plane and out-of-plane bulk states, respectively, and the red and green lines represent the two edge states, which are located at the two interfaces of I–II and II–I, respectively.

We can see that the edge modes in Fig. 4(c) are all A_0 modes. By mapping valley edge states from K' to K along $k_y = 0$ in first BZ, we take four symmetrical points on each line to check their modes and mechanical energy flow. It can be found that the valley pseudospin modes of points A_1 and A_2 in the range of $-\pi/2a \sim 0$ have an anticlockwise mechanical energy flow, while those of points B_1 and B_2 at the same position in the reciprocal space are clockwise. Similarly, the pseudospin modes on points $A_1{}'$ and $A_2{}'$ and points $B_1{}'$ and $B_2{}'$ are opposite to the above. Simulation results show that these two edge states have opposite propagation directions, and there exists a one-way propagation of pseudospin dependent elastic wave on the surface. Therefore, we will use this property to design the waveguides via using

Published under license by AIP Publishing

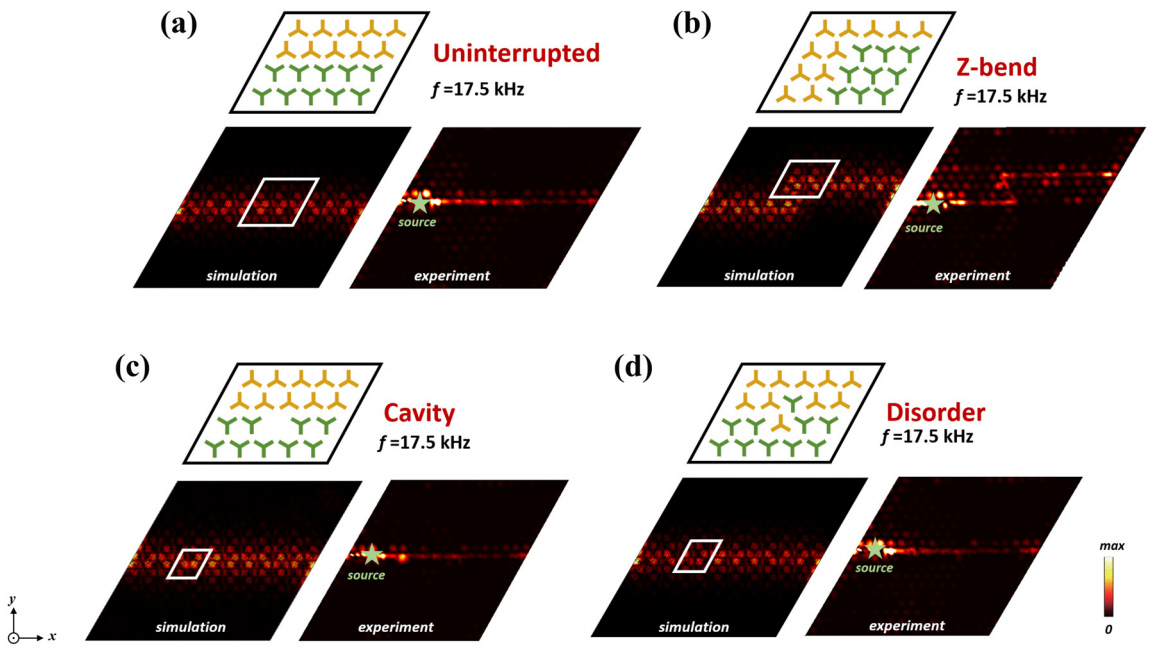

FIG. 5. Robustness of the topologically protected waveguide against different kinds of defects. (a) Uninterrupted; (b) Z-bend; (c) a cavity; and (d) a disordered area. White and black in the color bar denote maximum and minimum out-of-plane displacement $|w|$, respectively. The arrows indicate the direction of elastic wave propagation.

two different valley pseudospin edge states to achieve robust elastic wave propagation control.

The sample was fabricated according to the design described above to confirm the simulation results experimentally. The prisms with different φ were installed at the designated positions on the front and back sides of the aluminum plate. During the test, we used a shaker (4809, B&K), which was amplified by the power amplifier (2718, B&K), to excite the sample at the specified frequency. The shaker was fixed on the back side of the sample, and the exciting rod was connected with the quasi excitation point on the plate. The out-of-plane velocity wave field was measured by the scanning vibrometer (Polytec PSV-500) and recorded by the data acquisition. The picture of the experimental setup is shown in Fig. 5.

Based on the analysis of the valley pseudospin edge states in a supercell, we take its transmission characteristics of topological protection to construct the corresponding interface by combining the Type-I and Type-II PCPs. Our purposes are to verify the topological robustness of the structure with defects and to design relevant experiments to validate the simulation results, as shown in Fig. 6. Here, we design three kinds of defects: (I) Z-bend with sharp corners [Fig. 6(b)], (II) a

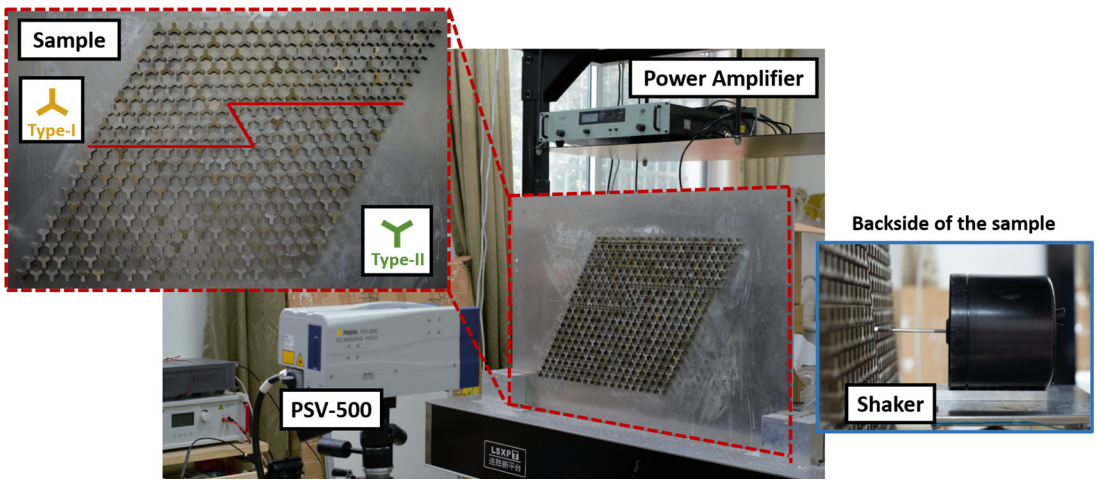

FIG. 6. Picture of the experimental setup.

Published under license by AIP Publishing

cavity [Fig. 6(c)], and (III) a disordered area [Fig. 6(d)]. For comparison, Fig. 6(a) shows an uninterrupted straight-line waveguide without any defects. The simulation and experimental results indicate that it can realize the stable transmission of the elastic wave. Figures 6(b)–6(d) are the waveguide channels with different defects, which show that, even if there are bends, cavities, and disordered areas in the path of waveguide, the elastic wave can still propagate along the waveguide robustly. It means this kind of structure has a strong ability of defect and bending immunity and can be an excellent candidate for elastic wave control devices. It is noted that the lower transmission observed in experiment than the simulated one should be due to the intrinsic material damping that was not considered in the simulations. In Sec. 6 of the supplementary material, we make a comparison between the simulation results for material with and without damping, which clearly indicates that the intrinsic material loss factor and damping can lead to a lower transmission, but the wave propagation characteristic of the overall design remains unchanged.

In addition, due to the reconfigurable property of the structure, we can use it to design a tunable topological elastic wave channel switcher and beam splitter combined with the immunity property for bending defects. As shown in Fig. 7(a), the blue region is a reconfigurable control region. We can construct waveguides with different channels via rotating the Y-shaped prisms in this area to realize the multi-channel propagation of elastic waves. When the upper and lower half areas of the control region are filled with Type-I and Type-II, respectively, the elastic waves will propagate along the straight line, as shown in Fig. 7(b), similar to that in Fig. 6(a). When exchanging the Type-I and Type-II areas, the elastic energy is partitioned equally into two parts and propagates into channel III and channel I, simultaneously, like Fig. 7(c), as a beam splitter. The reason why the elastic wave does not continue its straight-line channel is that the interfaces require elastic waves with opposite chirality, leading to the prevention of coupling. When the control region is adjusted to have only the Type-I or Type-II prisms, the wave output channel will be channel I or channel III, as indicated in Figs. 7(d) or 7(e). Moreover, we can install the electromagnetic control module under the prism and control it automatically by computer. In addition, the tunable region can be changed according to the actual needs to achieve more abundant multi-angle and multi-channel controllable and programmable waveguides.

In this paper, we constructed a reconfigurable thin phononic crystal plate with Y-shaped prisms arranged periodically on the top and bottom planes. By rotating the prisms, the A_0 mode part of the band structure realizes the opening and closing for the Dirac cone and the topological phase transition, thus realizing the valley Hall analogy of elastic waves. Based on this topological property, we can design the waveguide immune to defects and bendings, which reduces the energy loss in the process of elastic wave transmission and realizes robust elastic wave regulation. The strong robustness of the structure was verified by both experiments and simulations. In addition, we also used the genetic algorithm to optimize the structure to achieve the broadband effect and increase its practicability. The results obtained in this paper are of great significance to the practical applications of reconfigurable broadband elastic wave transmission.

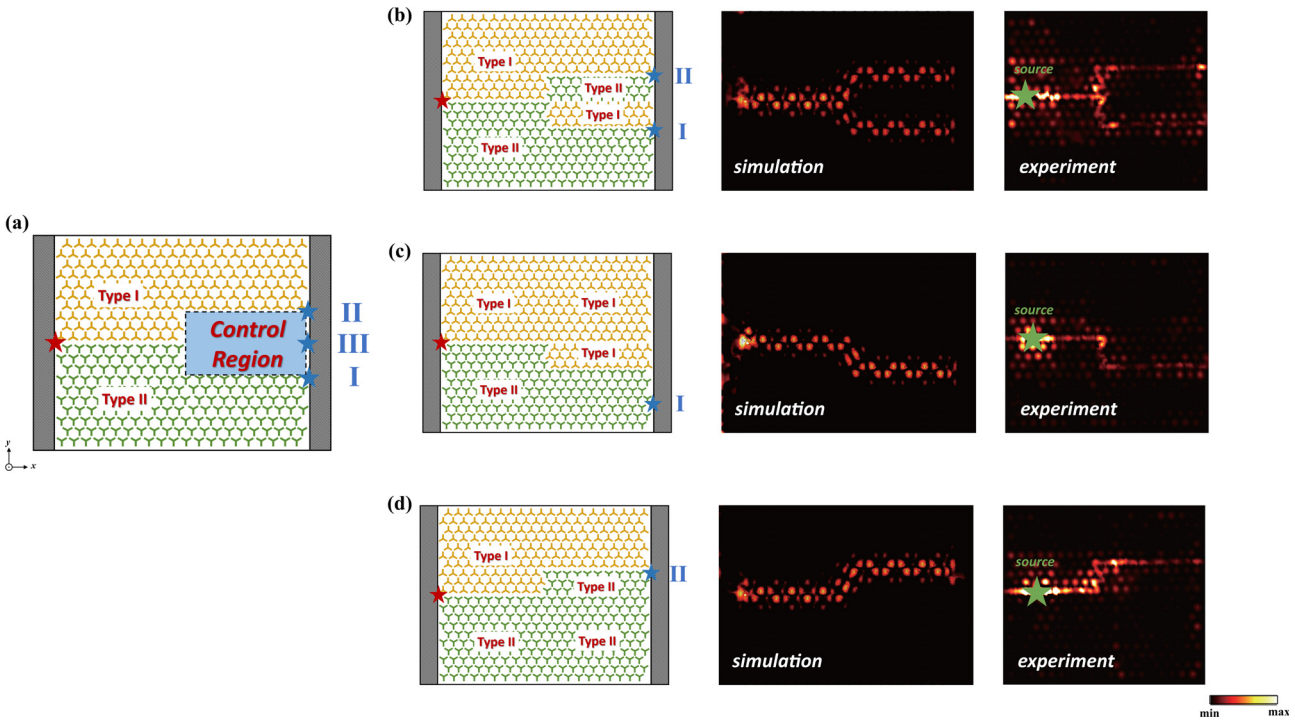

FIG. 7. (a) Reconfigurable topological elastic wave channel switcher or beam splitter, with the blue part being the tunable region, and different exits can be realized via rotating the Y-shaped prisms within this region; (b) elastic wave transmission through exits I and II at the same time; and (c) and (d) elastic wave transmission through exit I or II, showing the intrinsic symmetry in both simulation and experiment.

Published under license by AIP Publishing

See the supplementary material for the complete process of optimization, the calculation of the effective Hamiltonian, and the extra information of experiments.

AUTHORS' CONTRIBUTIONS

N.G. and S.Q. contributed equally to this work. N.G. and S.Q. conceived the idea and carried out the numerical simulations, N.G. and J.W. designed the experiments, J.W. and L.S. conducted the experiments, N.G., S.Q., and J.W. prepared this manuscript, and W.C. supervised the whole project. All the authors contributed to the analysis.

This work was supported by the National Natural Science Foundation of China (Nos. 11872329 and 11532001) and the Natural Science Foundation of Zhejiang Province (No. LD21A020001).

N. Gao and S. Qu sincerely thank Professor Ping Sheng of Hong Kong University of Science and Technology for helpful suggestions.

REFERENCES

[1]K. Graff, "Secondary," *Wave Motion in Elastic Solids* (Clarendon Press, Oxford, 1975).
[2]F. Deng, Y. Sun, X. Wang, R. Xue, Y. Li, H. Jiang, Y. Shi, K. Chang, and H. Chen, "Observation of valley-dependent beams in photonic graphene," Opt. Express **22**(19), 23605 (2014).
[3]T. Ma and G. Shvets, "Scattering-free edge states between heterogeneous photonic topological insulators," Phys. Rev. B **95**(16), 165102 (2017).
[4]J. Dong, X. Chen, H. Zhu, Y. Wang, and X. Zhang, "Valley photonic crystals for control of spin and topology," Nat. Mater. **16**(3), 298 (2017).
[5]F. Deng, Y. Li, Y. Sun, X. Wang, Z. Guo, Y. Shi, H. Jiang, K. Chang, and H. Chen, "Valley-dependent beams controlled by pseudomagnetic field in distorted photonic graphene," Opt. Lett. **40**(14), 3380 (2015).
[6]Z. Zhang, Y. Tian, Y. Cheng, X. Liu, and J. Christensen, "Experimental verification of acoustic pseudospin multipoles in a symmetry-broken snowflakelike topological insulator," Phys. Rev. B **96**(24), 241306 (2017).
[7]M. Xiao, G. Ma, Z. Yang, P. Sheng, Z. Zhang, and C. T. Chan, "Geometric phase and band inversion in periodic acoustic systems," Nat. Phys. **11**(3), 240 (2015).
[8]J. Lu, C. Qiu, L. Ye, X. Fan, M. Ke, F. Zhang, and Z. Liu, "Observation of topological valley transport of sound in sonic crystals," Nat. Phys. **13**(4), 369 (2017).
[9]J. Wang, Y. Huang, and W. Chen, "Tailoring edge and interface states in topological metastructures exhibiting the acoustic valley Hall effect," Sci. China: Phys., Mech. Astron. **63**(2), 224611 (2020).
[10]Z. Zhang, Y. Tian, Y. Cheng, Q. Wei, X. Liu, and J. Christensen, "Topological acoustic delay line," Phys. Rev. Appl. **9**(3), 034032 (2018).
[11]Z. Zhang, Q. Wei, Y. Cheng, T. Zhang, D. Wu, and X. Liu, "Topological creation of acoustic pseudospin multipoles in a flow-free symmetry-broken metamaterial lattice," Phys. Rev. Lett. **118**(8), 084303 (2017).
[12]J. Lu, C. Qiu, M. Ke, and Z. Liu, "Valley vortex states in sonic crystals," Phys. Rev. Lett. **116**(9), 093901 (2016).
[13]S. Huo, J. Chen, L. Feng, and H. Huang, "Pseudospins and topological edge states for fundamental antisymmetric Lamb modes in snowflakelike phononic crystal slabs," J. Acoust. Soc. Am. **146**(1), 729 (2019).
[14]S. Huo, J. Chen, H. Huang, and G. Huang, "Simultaneous multi-band valley-protected topological edge states of shear vertical wave in two-dimensional phononic crystals with veins," Sci. Rep. **7**(1), 1 (2017).
[15]E. Prodan and C. Prodan, "Topological phonon modes and their role in dynamic instability of microtubules," Phys. Rev. Lett. **103**(24), 248101 (2009).
[16]J. Vila, R. K. Pal, and M. Ruzzene, "Observation of topological valley modes in an elastic hexagonal lattice," Phys. Rev. B **96**(13), 134307 (2017).
[17]P. Wang, L. Lu, and K. Bertoldi, "Topological phononic crystals with one-way elastic edge waves," Phys. Rev. Lett. **115**(10), 104302 (2015).
[18]Q. Zhang, Y. Chen, K. Zhang, and G. Hu, "Dirac degeneracy and elastic topological valley modes induced by local resonant states," Phys. Rev. B **101**(1), 014101 (2020).
[19]W. Zhou, B. Wu, Z. Chen, W. Chen, C. Lim, and J. Reddy, "Actively controllable topological phase transition in homogeneous piezoelectric rod system," J. Mech. Phys. Solids **137**, 103824 (2020).
[20]H. Chen, H. Nassar, and G. Huang, "A study of topological effects in 1D and 2D mechanical lattices," J. Mech. Phys. Solids **117**, 22 (2018).
[21]H. Chen, H. Nassar, A. N. Norris, G. Hu, and G. Huang, "Elastic quantum spin Hall effect in kagome lattices," Phys. Rev. B **98**(9), 094302 (2018).
[22]H. Chen, L. Yao, H. Nassar, and G. Huang, "Mechanical quantum Hall effect in time-modulated elastic materials," Phys. Rev. Appl. **11**(4), 044029 (2019).
[23]Y. Chen, X. Liu, and G. Hu, "Topological phase transition in mechanical honeycomb lattice," J. Mech. Phys. Solids **122**, 54 (2019).
[24]Z. G. Chen and Y. Wu, "Tunable topological phononic crystals," Phys. Rev. Appl. **5**(5), 054021 (2016).
[25]A. B. Khanikaev, R. Fleury, S. H. Mousavi, and A. Alu, "Topologically robust sound propagation in an angular-momentum-biased graphene-like resonator lattice," Nat. Commun. **6**(1), 1 (2015).
[26]R. K. Pal and M. Ruzzene, "Edge waves in plates with resonators: An elastic analogue of the quantum valley Hall effect," New J. Phys. **19**(2), 025001 (2017).
[27]Q. Zhang, Y. Chen, K. Zhang, and G. Hu, "Programmable elastic valley Hall insulator with tunable interface propagation routes," Extreme Mech. Lett. **28**, 76 (2019).
[28]P. Wang, Y. Zheng, M. C. Fernandes, Y. Sun, K. Xu, S. Sun, S. H. Kang, V. Tournat, and K. Bertoldi, "Harnessing geometric frustration to form band gaps in acoustic channel lattices," Phys. Rev. Lett. **118**(8), 084302 (2017).
[29]S. Yu, C. He, Z. Wang, F.-K. Liu, X. Sun, Z. Li, H. Lu, M. Lu, X. Liu, and Y. Chen, "Elastic pseudospin transport for integratable topological phononic circuits," Nat. Commun. **9**(1), 3072 (2018).
[30]T. Liu and F. Semperlotti, "Tunable acoustic valley–Hall edge states in reconfigurable phononic elastic waveguides," Phys. Rev. Appl. **9**(1), 014001 (2018).
[31]J. Wang and J. Mei, "Topological valley-chiral edge states of Lamb waves in elastic thin plates," Appl. Phys. Express **11**(5), 057302 (2018).
[32]Z. Wang, Q. Wei, H. Xu, and D. Wu, "A higher-order topological insulator with wide bandgaps in Lamb-wave systems," J. Appl. Phys. **127**(7), 075105 (2020).
[33]M. Yan, J. Lu, F. Li, W. Deng, X. Huang, J. Ma, and Z. Liu, "On-chip valley topological materials for elastic wave manipulation," Nat. Mater. **17**(11), 993 (2018).
[34]Z. Du, H. Chen, and G. Huang, "Optimal quantum valley Hall insulators by rationally engineering Berry curvature and band structure," J. Mech. Phys. Solids **135**, 103784 (2020).
[35]D. Whitley, "A genetic algorithm tutorial," Stat. Comput. **4**(2), 65 (1994).
[36]A. S. Gliozzi, M. Miniaci, F. Bosia, N. M. Pugno, and M. Scalerandi, "Metamaterials-based sensor to detect and locate nonlinear elastic sources," Appl. Phys. Lett. **107**(16), 161902 (2015).
[37]M. Miniaci, A. S. Gliozzi, B. Morvan, A. Krushynska, F. Bosia, M. Scalerandi, and N. M. Pugno, "Proof of concept for an ultrasensitive technique to detect and localize sources of elastic nonlinearity using phononic crystals," Phys. Rev. Lett. **118**(21), 214301 (2017).
[38]M. Kurosu, D. Hatanaka, K. Onomitsu, and H. Yamaguchi, "On-chip temporal focusing of elastic waves in a phononic crystal waveguide," Nat. Commun. **9**(1), 1331 (2018).

Published under license by AIP Publishing

View publication stats